

Global Data Products for Sustainable Development 2025

International Research Center of Big Data for Sustainable Development Goals
Beijing · China

Global Data Products for Sustainable Development

2025



CONTENTS

P.04 Global 30-m land cover dynamic monitoring product with a fine classification system from 1985 to 2022 (GLC_FCS30D_1985-2022)

Support SDGs： SDG 2; SDG 13; SDG 15

P.08 Global human thermal stress index product from 2000 to 2024 (HiGTS_2000-2024)

Support SDGs：SDG 3; SDG 11; SDG 13

P.12 Global industrial heat source data product from 2012 to 2023 (GIHS_2012-2023)

Support SDGs：SDG 7; SDG 8; SDG 9; SDG 12

P.16 Global 10-m spatial distribution of mangroves in 2020 (HGMF_10m_2020)

Support SDGs：SDG 6; SDG 13; SDG 14;SDG 15

P.20 Global 30-m annual afforestation monitoring product from 1990 to 2024 (GAAM_30m_1990-2024)

Support SDGs：SDG 15

P.24 Global 30-m marine raft aquaculture data product in 2010, 2020, and 2024 (GOFAR_30m_2010/2020/2024)

Support SDGs：SDG 14

P.28 Global 1-km soil moisture data product in 2020, 2021, and 2024 (GL_SSM_1km_2020/2021/2024)

Support SDGs：SDG 2； SDG 15

P.32 Global 1-km aerosol optical depth data product in 2020, 2021, and 2024 (GL_AOD_1km_2020/2021/2024)

Support SDGs：SDG 11

P.36 Global 1-km latent heat flux data product in 2020, 2021, and 2024 (GL_LE_1km_2020/2021/2024)

Support SDGs：SDG 2； SDG 6； SDG 15



Global 30-m land cover dynamic monitoring product with a fine classification system from 1985 to 2022 (GLC_FCS30D_1985-2022)

Product Summary

"Land cover" refers to the synthesis of various feature types and their natural attributes and characteristics on the Earth's land surface, including surface vegetation, soil, lakes, swamps and wetlands, snow and ice, and various buildings, with specific temporal and spatial attributes.

The dynamic monitoring of land cover is crucial for global environmental research, providing key data to support global ecological assessment and policy making. The GLC_FCS30D_1985-2022 product leverages both domestic and international satellite remote sensing data to classify the global land surface into 27 fine land cover categories, revealing the spatial distribution of land and its changes over time from 1985 to 2022. It adopts continuous change monitoring technology to provide datasets on global land cover dynamics at 30 m resolution.

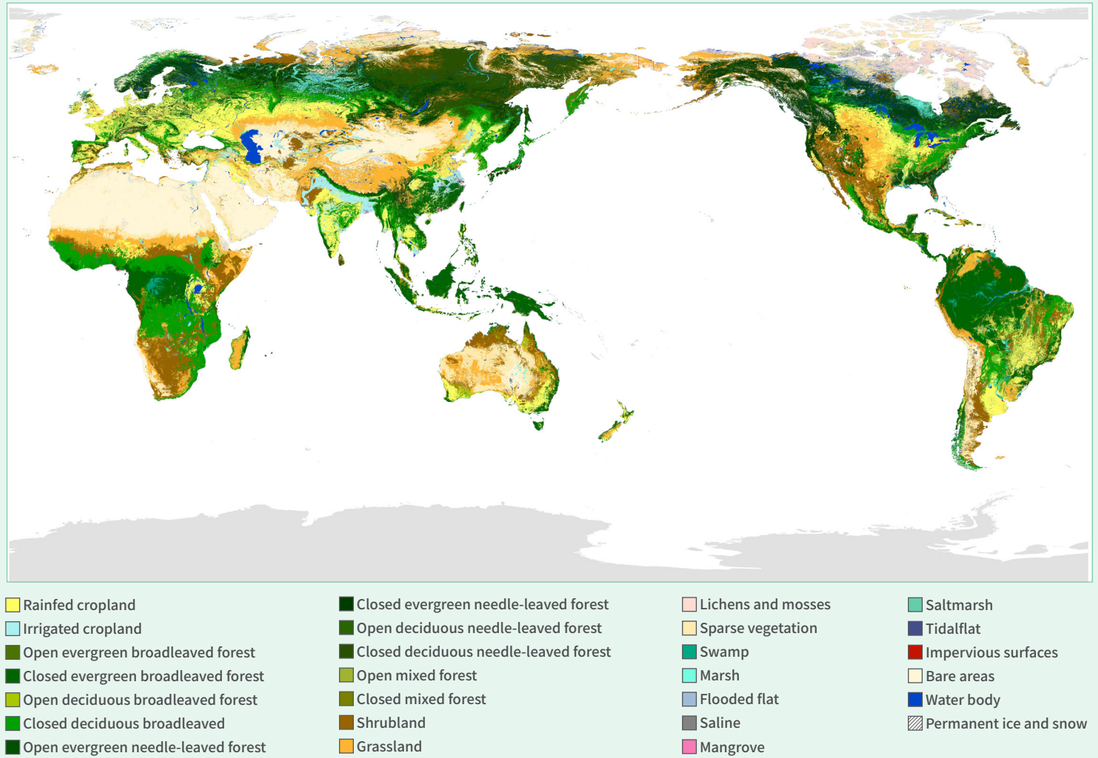
Temporal: The dataset covers the period from 1985 to 2022 with 26 time steps. Data were collected at 5-year intervals before 2000 and annually from 2000 onward.

Geo Scope: The dataset covers a geographical extent from 60° S to 80° N in latitude, with a spatial resolution of 0.0002695° (equivalent to 30 m in the equatorial region).



Support SDGs: SDG 2 Zero hunger
SDG 13 Climate action
SDG 15 Life on land

Overview of the global 30-m land cover dynamic monitoring product in 2022



Methods

This product is developed using a combined full-time-series change detection and dynamic updating strategy, which fully utilizes all available Landsat observation data to ensure reliable land cover change monitoring. Specifically, it captures the spatiotemporal information of per-pixel land cover changes using a continuous change detection model and full-time-series Landsat observations. Next, we combined the change detection results with the proposed sample refinement algorithm to build a high-confidence training sample library. Further, the land cover information of these changed pixels is dynamically updated using a local adaptive classification model, multi-temporal Landsat observations, and prior GLC_FCS30 land cover maps in 2020. Lastly, the land cover information of the changed pixels is further improved by adopting a temporal consistency optimization algorithm.

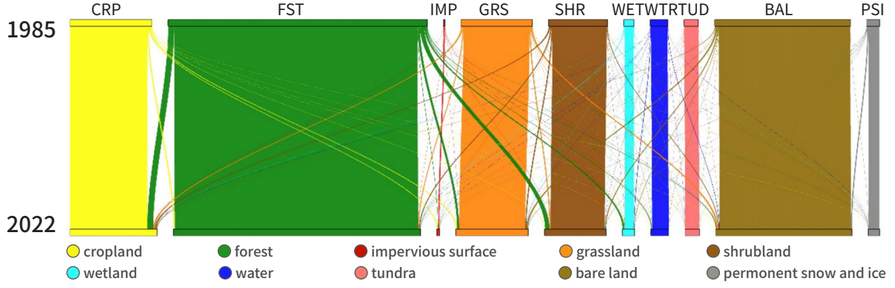
Accuracy assessment

The product was validated using 84 526 globally distributed validation samples in 2020, and the results indicated that the GLC_FCS30D achieved an overall accuracy of 80.88% (±0.27%). Meanwhile, two third-party time-series validation datasets in the United States and the European Union were also collected, and the results showed that the GLC_FCS30D dataset showed significant time-series stability, with average accuracies of 79.50% (±0.50%) and 81.91% (±0.09%) in the two regions, respectively.



Scientific Results:

The statistical results show that between 1985 and 2022, changes in forests and farmland dominated global land cover changes, with a net decrease of about 2.68 million square kilometers in the global forest area and a net increase of about 1.03 million square kilometers in cultivated land area. These changes mainly occurred in the Amazon region of South America, the Congo in Africa, and the tropical rainforests of Southeast Asia, where most forests have been converted into cropland. For example, most tropical forests of Southeast Asia have been converted into oil palm plantations. Other land cover types also experienced changes; the most significant net increase in impervious surfaces was about 620 000 square kilometers, with a 70.90% increase in impervious surfaces in cropland and a 9.13% increase in forests. Cropland expansion occurred primarily in peri-urban flat areas, while forest occupancy was mainly in North America and Oceania.



Product Details

The product uses the WGS84 coordinate system, with longitude and latitude projection (EPSG:4326), and a resolution of 0.0002695° (approximately 30-m) for block output. The output format is GeoTIFF. Each block covers 5° ×5° , with a size of approximately 18 554 pixels×18 554 pixels, totaling 961 blocks. Each image block is encoded according to the longitude and latitude in its upper-left corner.

▪ **Corresponding Authors:** Liangyun Liu, liuly@radi.ac.cn; Xiao Zhang, zhangxiao01@aircas.ac.cn

▪ **References:**

1. Xiao Zhang, Tingting Zhao, Hong Xu, et al. 2024. GLC_FCS30D: the first global 30m land-cover dynamics monitoring product with a fine classification system for the period from 1985 to 2022 generated using dense-time-series Landsat imagery and the continuous change-detection method. Earth System Science Data, 16, 1353-1381. https://doi.org/10.5194/essd-16-1353-2024.

2. Tingting Zhao, Xiao Zhang, Yuan Gao, et al. 2023. Assessing the Accuracy and Consistency of Six Fine-Resolution Global Land Cover Products Using a Novel Stratified Random Sampling Validation Dataset. Remote Sensing, 15, 2285. https://doi.org/10.3390/rs15092285.

▪ **Data Citation:** Xiao Zhang, Liangyun Liu. Global 30-m land cover dynamic monitoring product with a fine classiffcation system from 1985 to 2022 (GLC_FCS30D_1985-2022), Beijing: International Research Center of Big Data for Sustainable Development Goals (CBAS), 2026. doi: 10.12237/casearth.689ecf47913dfd1b2d6cb83d

▪ **Product URL:** http://data.casearth.cn/thematic/2025

▪ **Citation and Disclaimer for Data Use:** Users of this product shall clearly indicate the source and the authors of "Global 30-m land cover dynamic monitoring product with a fine classification system from 1985 to 2022 (GLC_FCS30D_1985-2022)" in all forms of their research output, including, but not limited to, published and unpublished papers/reports, theses, monographs, and data products generated by using this data product, and shall cite the corresponding references. The data producers shall not be liable for any loss arising from the use of this product. The boundaries and markings on the maps do not represent any official opinion or endorsement by the data producers.

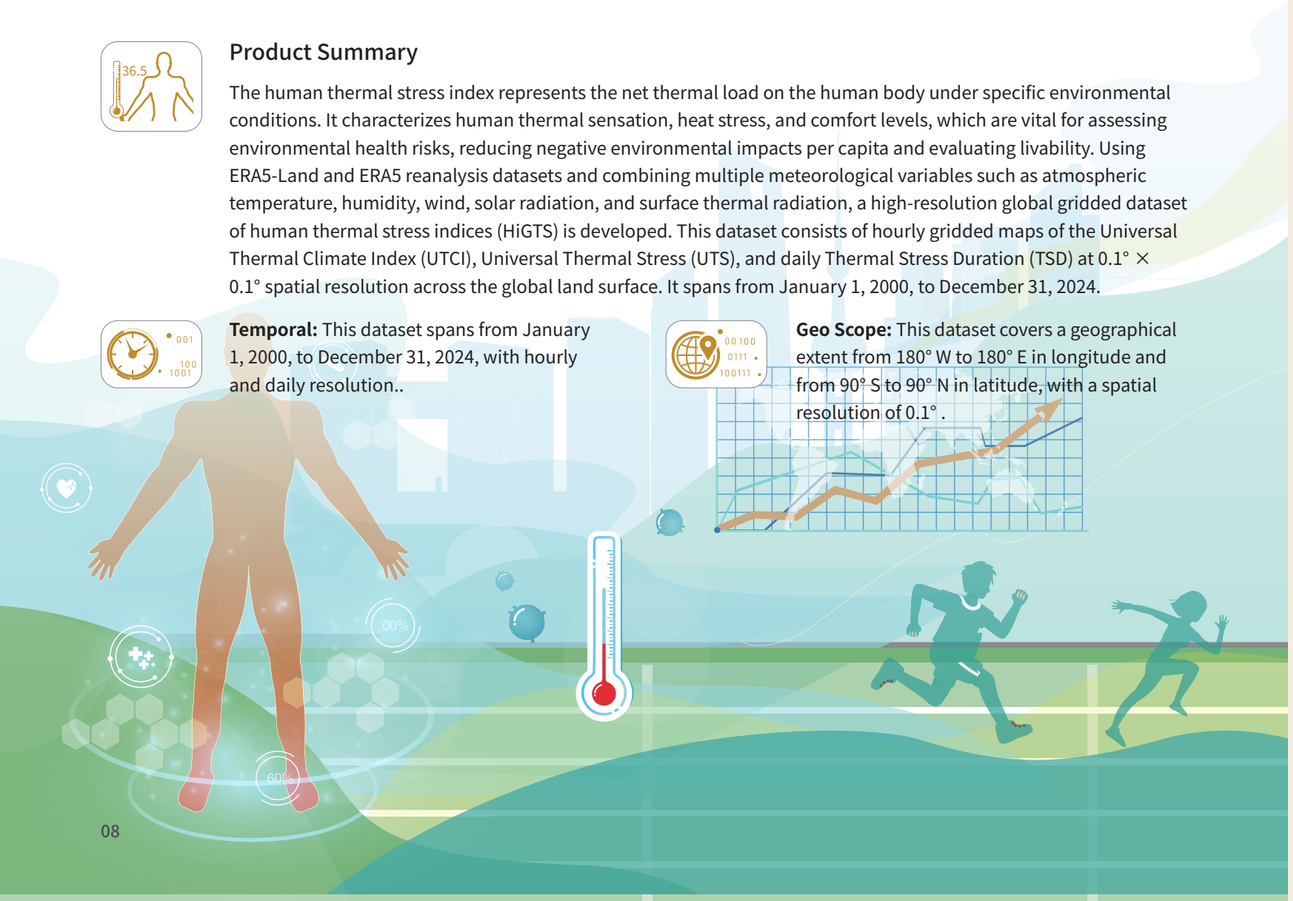
Global human thermal stress index product from 2000 to 2024 (HiGTS_2000-2024)

Product Summary

The human thermal stress index represents the net thermal load on the human body under specific environmental conditions. It characterizes human thermal sensation, heat stress, and comfort levels, which are vital for assessing environmental health risks, reducing negative environmental impacts per capita and evaluating livability. Using ERA5-Land and ERA5 reanalysis datasets and combining multiple meteorological variables such as atmospheric temperature, humidity, wind, solar radiation, and surface thermal radiation, a high-resolution global gridded dataset of human thermal stress indices (HiGTS) is developed. This dataset consists of hourly gridded maps of the Universal Thermal Climate Index (UTCI), Universal Thermal Stress (UTS), and daily Thermal Stress Duration (TSD) at 0.1° × 0.1° spatial resolution across the global land surface. It spans from January 1, 2000, to December 31, 2024.

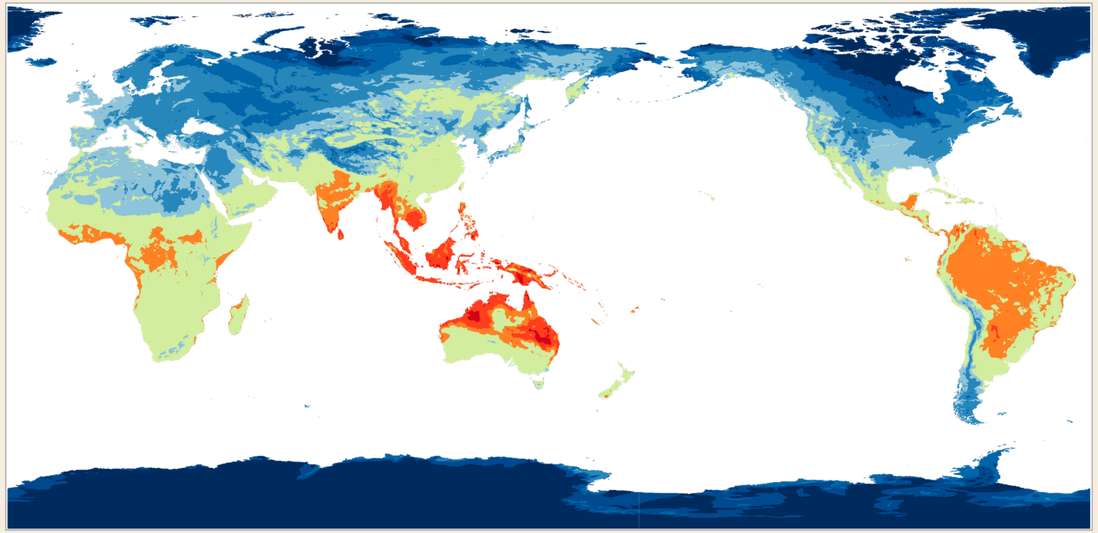
Temporal: This dataset spans from January 1, 2000, to December 31, 2024, with hourly and daily resolution..

Geo Scope: This dataset covers a geographical extent from 180° W to 180° E in longitude and from 90° S to 90° N in latitude, with a spatial resolution of 0.1° .



Support SDGs: SDG 3 Good Health and Well-being
SDG 11 Sustainable Cities and Communities
SDG 13 Climate Action

Thermal Stress over the global land surface at 2024-03-20T03Z (vernal equinox)



	UTCI/° C	Category	Abbreviation	UTS value
	Above 46	Extreme heat stress	ehs	4
	38 to 46	Very strong heat stress	vshs	3
	32 to 38	Strong heat stress	shs	2
	26 to 32	Moderate heat stress	mhs	1
	9 to 26	No thermal stress	nts	0

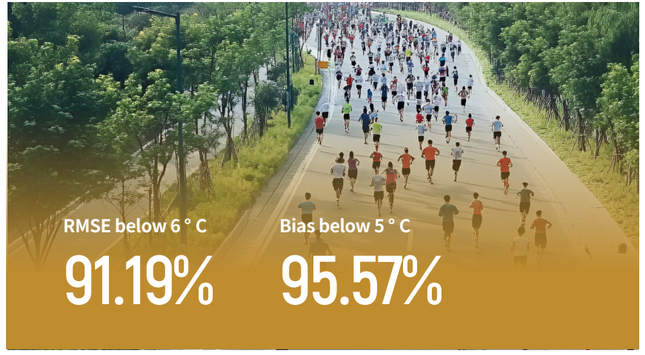
	UTCI/° C	Category	Abbreviation	UTS value
	0 to 9	Slight cold stress	slcs	-1
	-13 to 0	Moderate cold stress	mcs	-2
	-13 to -27	Strong cold stress	scs	-3
	-27 to -40	Very strong cold stress	vscs	-4
	Below -40	Extreme cold stress	ecs	-5

Methods

Using variables from ERA5-Land and ERA5 reanalysis datasets, such as solar radiation, surface thermal radiation, atmospheric temperature, dewpoint temperature, and wind, the UTCI, UTS, and TSD are calculated using the UTCI model and TSD calculation methods. The UTCI is a multivariate parameter describing the synergistic heat exchanges between the thermal environment and the human body, representing the equivalent temperature influenced by multiple meteorological factors, such as atmospheric temperature, humidity, wind speed, and Mean Radiant Temperature (MRT), with the unit ° C. The UTS is derived from UTCI equivalent temperatures in terms of thermal stress, divided into 10 categories to indicate different levels of thermal stress. The TSD is the cumulative hours of different thermal stress values within a specific period and contains ten variables measured in hours.

Accuracy assessment

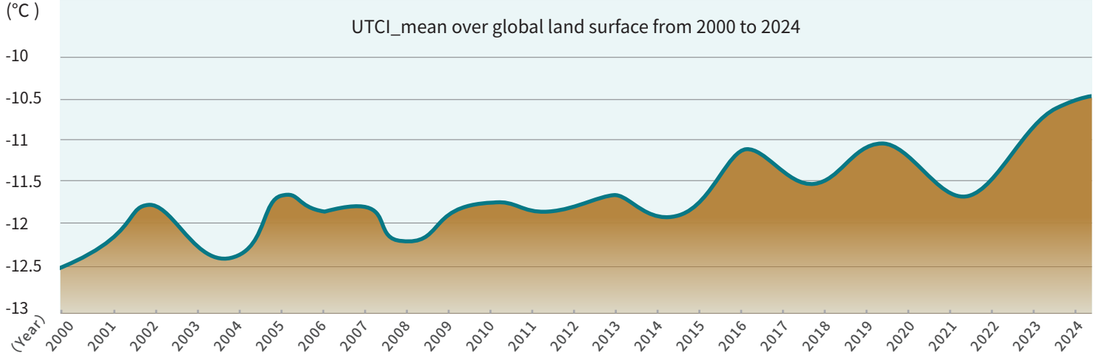
The product implemented quality control throughout the production process and was technically compared with two other high temporal resolution datasets of human thermal stress: HiTiSEA and ERA5-HEAT. The daily mean of UTCI in HiGTS and the UTCI_mean in HiTiSEA have almost identical values, with RMSE below 0.2° C and bias below 0.09° C. The average RMSE and bias of HiGTS and ERA5-HEAT are 1.79° C and 0.77° C, respectively. The percentage of grids with an RMSE below 5° C exceeds 98.84%, and that with a bias below 5° C exceeds 99.50%.



The HiGTS was compared against observations from the global hourly meteorological stations of the Integrated Surface Database (ISD) provided by the National Centers for Environmental Information (NCEI). The average RMSE and bias for HiGTS and ISD stations are 3.93° C and -0.65° C, respectively. The percentage of stations with an RMSE below 6° C is 91.19%, and that with a bias below 5° C is 95.57%.

Scientific Results:

The yearly mean values of UTCI over the global land surface from 2000 to 2024 were calculated using the long time-series HiGTS-2000_2024 product. The global human thermal stress showed an overall fluctuating upward trend, with UTCI_mean over the global land surface increasing by about 1.5° C during the 25 years and reaching its highest value in 2024. As an equivalent temperature of human thermal stress influenced by multiple meteorological variables, such as atmospheric temperature, humidity, wind speed, and average radiation temperature, UTCI exhibits greater fluctuations than atmospheric temperature alone, indicating that the thermal stress felt by the human body is more sensitive to climate change.



Product Details

This product uses a regular latitude-longitude grid for data storage, with NetCDF (.nc) as the output format. Each thermal stress metric is saved as a daily NetCDF file named Metric_YYYYMMDD.nc (where Metric is the name of the metric and YYYYMMDD refers to the date). The dataset includes 27 396 files, totaling 1.28TB.

▪ **Corresponding Authors:** Hongdeng Jian, jianhd@aircas.ac.cn

▪ **References:**

1. Hongdeng Jian, Zhenzhen Yan, Xiangtao Fan, et al. 2024. A high temporal resolution global gridded dataset of human thermal stress metrics. Scientific Data, 11, 1116. https://doi.org/10.1038/s41597-024-03966-x.

▪ **Data Citation:** Hongdeng Jian, Zhenzhen Yan, Xiangtao Fan. Global human thermal stress index product from 2000 to 2024 (HiGTS_2000-2024) , Beijing: International Research Center of Big Data for Sustainable Development Goals (CBAS), 2026. doi: 10.12237/casearth.689ed08a913dfd1b2d6cb83e

▪ **Product URL:** http://data.casearth.cn/thematic/2025

▪ **Citation and Disclaimer for Data Use:** Users of this product shall clearly indicate the source and the authors of "Global human thermal stress index product from 2000 to 2024 (HiGTS_2000-2024)" in all forms of their research output, including, but not limited to, published and unpublished papers/reports, theses, monographs, and data products generated by using this data product, and shall cite the corresponding references. The data producers shall not be liable for any loss arising from the use of this product. The boundaries and markings on the maps do not represent any official opinion or endorsement by the data producers.

Global industrial heat source data product from 2012 to 2023 (GIHS_2012-2023)

Product Summary

Industrial heat sources (IHS) refer to areas with concentrated thermal radiation identified via remote sensing. They include industrial firms such as cement plants, oil refineries and exploration sites, and chemical processing plants with surface areas exceeding 16 m^2 and operational cycles longer than 90 days that display distinct thermal radiation signatures. They demand a large amount of primary or secondary energy during manufacturing and release massive heat radiation and atmospheric pollutants (e.g., CO_2, CH_4, CO, NO_2, SO_2) into the air (Ma et al.,2024). These firms understand that the complex interplay between human activities and global changes, including air pollution and the intensification of global warming, requires recognizing the significance of IHS as a crucial source of knowledge. Changes in IHS contribute to understanding global environmental changes and regional economic development, ultimately impacting climate change.

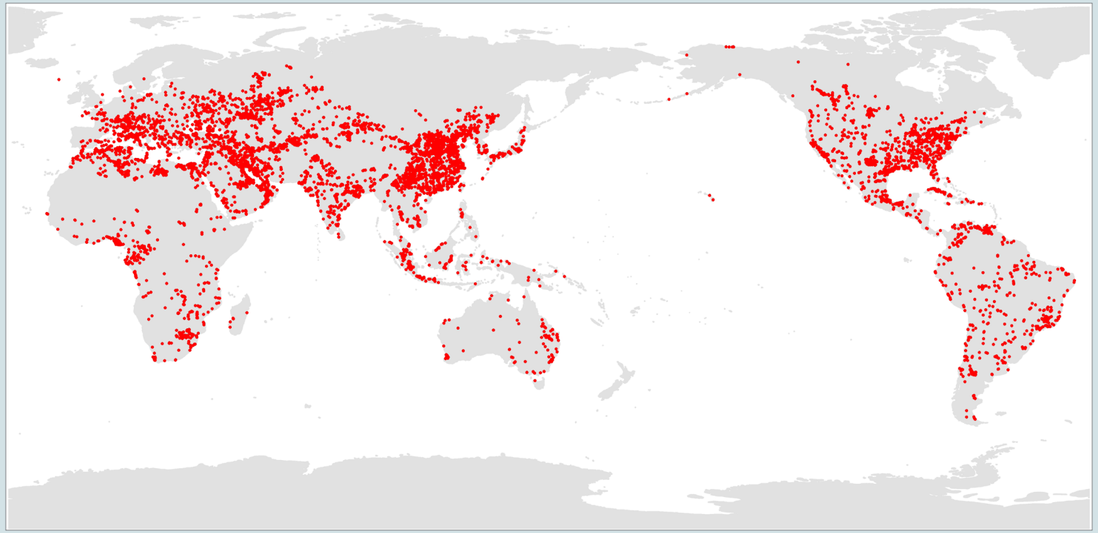
Temporal: The product is generated using thermal anomaly data and active fire point data from NPP-VIIRS sensors collected from 2012 to 2023, consisting of 12 datasets with a yearly temporal resolution.

Geo Scope: The product covers a geographical extent from 180° W to 180° E in longitude and from 80° S to 80° N in latitude, with industrial heat sources detectable at a minimum size of 16 m^2.

Support SDGs: SDG 7 Affordable and clean energy
SDG 8 Decent work and economic growth
SDG 9 Industry, innovation and infrastructure
SDG 12 Responsible consumption and production product



Global heat sources in 2023



Industrial Heat Source

Methods

The GIHS product is built on global long-term thermal anomaly datasets from 2012 to 2023, leveraging the "fixed location, continuous time" spatiotemporal characteristics of industrial heat sources. It adopts an identification method that combines spatiotemporal density segmentation and machine learning, validated through high-resolution remote sensing data, manual verification, and field surveys. The data sources include NPP-VIIRS (Suomi National Polar-orbiting Partnership, Visible Infrared Imaging Radiometer Suite) 375m thermal anomalies/ active fire product (ACF), GF-1 and GF-6 satellite imagery, among others.

A density-based spatiotemporal clustering model integrating machine learning was used. First, ACF data from 2012 to 2023 were acquired and pre-processed. Next, an adaptive K-means algorithm was applied to generate the initial GIHS dataset. The final GIHS for 2012 and 2023 was derived using max-nighttime light data. Finally, GIHS from 2012 to 2023 was derived using max-nighttime light data, and validated through high-resolution imagery, global reference datasets, and field surveys.

Accuracy assessment

Using GF-1/6 high-resolution imagery, global reference datasets, and field survey data as validation sources, each of the 26 240 GIHS objects from 2012 to 2023 was manually verified. The overall accuracy reached 93.34%.



▪ **Corresponding Author:** Caihong Ma, mach@aircas.ac.cn

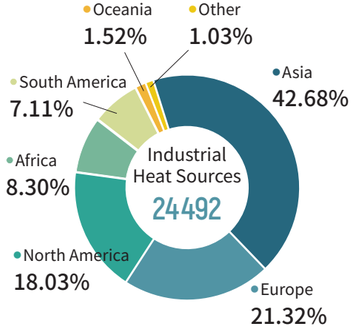
▪ **References:**

1. Caihong Ma, Tianzhu Li, Xin Sui, et al. 2024. Annual dynamics of global remote industrial heat sources dataset from 2012 to 2021. Scientific Data, 11,631. https://doi.org/10.1038/s41597-024-03461-3.

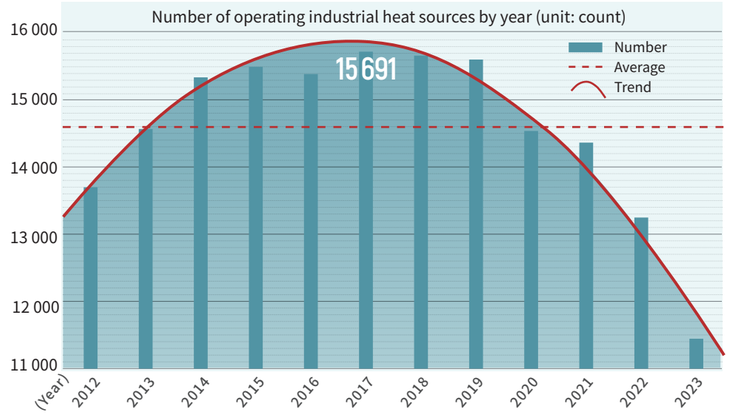
2. Caihong Ma, Jin Yang, Fu Chen, et al. 2018. Assessing Heavy Industrial Heat Source Distribution in China Using Real-Time VIIRS Active Fire/ Hotspot Data. Sustainability, 10,4419. https://doi.org/10.3390/su10124419.

Scientific Results:

From 2012 to 2023, the number of global industrial heat sources first increased and then decreased, reaching a peak in 2017. After 2018, it declined, reaching a low in 2023—a 27.13% decrease from the 2017 peak. Industrial heat sources are spatially concentrated in Asia, Europe, and North America, with Asia accounting for 42.68% (largest) and Oceania 1.52% (smallest). Among 193 UN member states, the top five countries by terrestrial industrial heat source count in 2023 constituted 52% of the global total. 115 countries had fewer than 10 industrial heat sources—including 44 with none—highlighting significant disparities in global industrialization progress.



Global Industrial Heat Sources: Continental Statistics



Product Details

This product adopts the WGS84 coordinate system and latitude longitude projection (EPSG: 4326), with an output file format of shapefile and a total of 26 240 polygon vector data.

▪ **Data Citation:** Caihong Ma. Global industrial heat source data product from 2012 to 2023 (GIHS_2012-2023), Beijing: International Research Center of Big Data for Sustainable Development Goals (CBAS), 2026. doi:10.12237/casearth.68be4f199418b437b222236b

▪ **Product URL:**http://data.casearth.cn/thematic/2025

▪ **Citation and Disclaimer for Data Use:** Users of this product shall clearly indicate the source and the authors of "Global industrial heat source data product from 2012 to 2023 (GIHS_2012-2023)" in all forms of their research output, including, but not limited to, published and unpublished papers/reports, theses, monographs, and data products generated by using this data product, and shall cite the corresponding references. The data producers shall not be liable for any loss arising from the use of this product. The boundaries and markings on the maps do not represent any official opinion or endorsement by the data producers.

Global 10-m spatial distribution of mangroves in 2020 (HGMF_10m_2020)

Product Summary

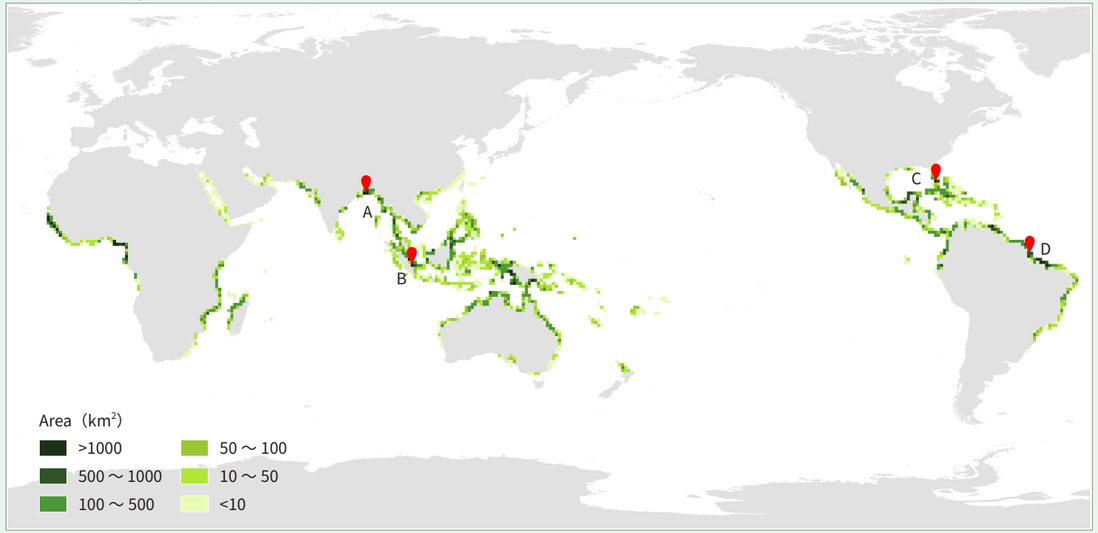
Mangrove forests are woody wetland plant communities that thrive in tropical and subtropical coastal intertidal zones and river estuaries. As one of the most productive and biodiverse ecosystems on Earth, mangroves play a vital role in coastal protection, land accretion, carbon sequestration, and biodiversity conservation. As a key component of coastal blue carbon ecosystems, mangroves are essential for climate change mitigation.The spatial distribution and patch structure of mangroves serve as key ecological indicators for evaluating coastal ecological security and sustainable development.

Temporal: The product is generated using approximately 124 000 cloud-free (cloud cover <2%) Sentinel-2 images acquired globally across mangrove regions between January 1 and December 31, 2020.

Geo Scope: The dataset covers all mangrove growing regions worldwide, ranging from 180° W to 180° E in longitude and from 40° S to 30° N in latitude, with a spatial resolution of 0.00008983° (equivalent to 10 m at the equator). It covers coastal areas in Asia, Africa, North America, South America, and Oceania.

Support SDGs: SDG 6 Clean water and sanitation
SDG 13 Climate action
SDG 14 Life below water
SDG 15 Life on land

Global Mangrove Area Levels in 2020 (Statistics Based on 1° Grid Cells, Derived from 10-m Resolution Satellite Image Interpretation)



Mangrove forests

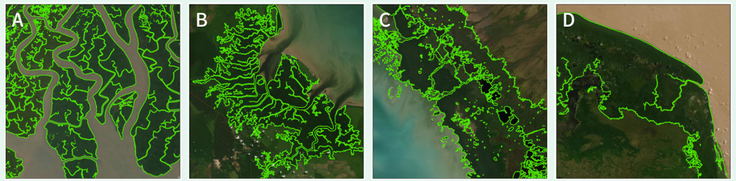
Partial mangrove area

A . Sundarbans along the Bay of Bengal

B . Sembilang National Park in Indonesia's South Sumatra Province

C . Everglades National Park, Florida, the United States

D . The estuary of the Amazon River, Brazil



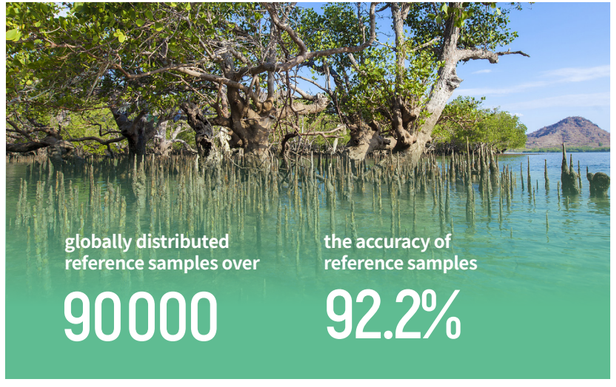
Methods

The product was developed using dense time-series remote sensing data and an object-oriented machine learning approach, enabling comprehensive identification and extraction of mangrove forests at the global scale. To define the study area's spatial extent, publicly available global mangrove datasets with varying temporal and spatial resolutions, such as the Global Mangrove Watch, were integrated to delineate core mangrove distribution zones.A 5 km buffer was applied to account for intertidal regions and transitional ecosystems. By leveraging the high revisit frequency of Sentinel-2 imagery, a high-precision and robust automated compositing method was developed to generate cloud-free, low-tide composite images for tropical and subtropical coastal regions. Using object-oriented image analysis and a random forest classifier, the spatial extent of mangrove patches was identified, resulting in the 2020 global mangrove spatial distribution product at 10 m resolution.

The extracted mangrove patches display complete spatial morphology and clearly defined boundaries, including ecological and geographical features such as tidal creeks and canopy gaps.

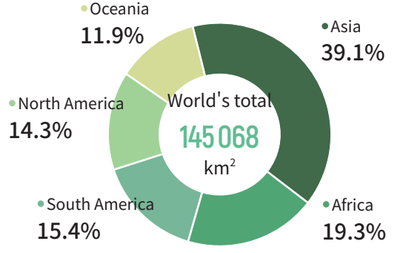
Accuracy assessment

A systematic validation of over 90 000 globally distributed reference samples shows that the product achieves an overall accuracy of 92.2%, with user and producer accuracies for mangrove classification reaching 85.4% and 85.2%, respectively. It demonstrates enhanced capability in detecting small and fragmented mangrove patches. Compared with seven major existing global mangrove datasets, including GMFD, the GMW series (v2.0, v2.5, v3.0), CGMFC-21, LREIS_GLOBALMANGROVE, and GMF30_2000–2020, this product offers higher spatial resolution, improved patch integrity, and more precise boundaries.

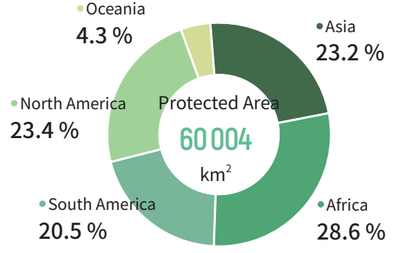


Scientific Results:

In 2020, the total area of global mangrove forests was estimated at 145 068 km², with 96% located in tropical regions—highlighting its typical association with coastal tropical ecosystems. Asia had the largest portion of mangroves, covering 56 722 km² (39.1% of the global total), followed by Africa (27 998 km², 19.3%), South America (22 340 km², 15.4%), North America (20 745 km², 14.3%), and Oceania (17 263 km², 11.9%).



Area and proportion of mangrove forests on each continent



Area and proportion of protected mangrove forests on each continent

Product Details

This product adopts the WGS 84 geographic coordinate system with a geographic (EPSG:4326) projection and a grid resolution of 0.00008983° (approximately 10 m). The data are provided in GeoTIFF format and divided into 223 tiles, each covering a 5° × 5° area with a pixel size of approximately 55 660 × 55 660. Each tile is encoded based on the longitude and latitude of its upper-left corner.

▪ **Corresponding Author:** Mingming Jia, jiamingming@iga.ac.cn

▪ **References:**

1. Mingming Jia, Zongming Wang, Dehua Mao, et al. 2023. Mapping global distribution of mangrove forests at 10-m resolution. Science Bulletin, 68, 1306-1316. https://doi.org/10.1016/j.scib.2023.05.004.

▪ **Data Citation:** Mingming Jia. Global 10m spatial distribution of mangroves in 2020 (HGMF_10m_2020), Beijing: International Research Center of Big Data for Sustainable Development Goals (CBAS), 2026. doi: 10.12237/casearth.6a87f2312e35784b06034964

▪ **Product URL:**http://data.casearth.cn/thematic/2025

▪ **Citation and Disclaimer for Data Use:**Users of this product shall clearly indicate the source and the authors of "Global 10-m spatial distribution of mangroves in 2020 (HGMF_10m_2020)" in all forms of their research output, including, but not limited to, published and unpublished papers, reports, theses, monographs, and data products generated by using this data product, and shall cite the corresponding references. The data producers shall not be liable for any loss arising from the use of this product. The boundaries and markings on the maps do not represent any official opinion or endorsement by the data producers.

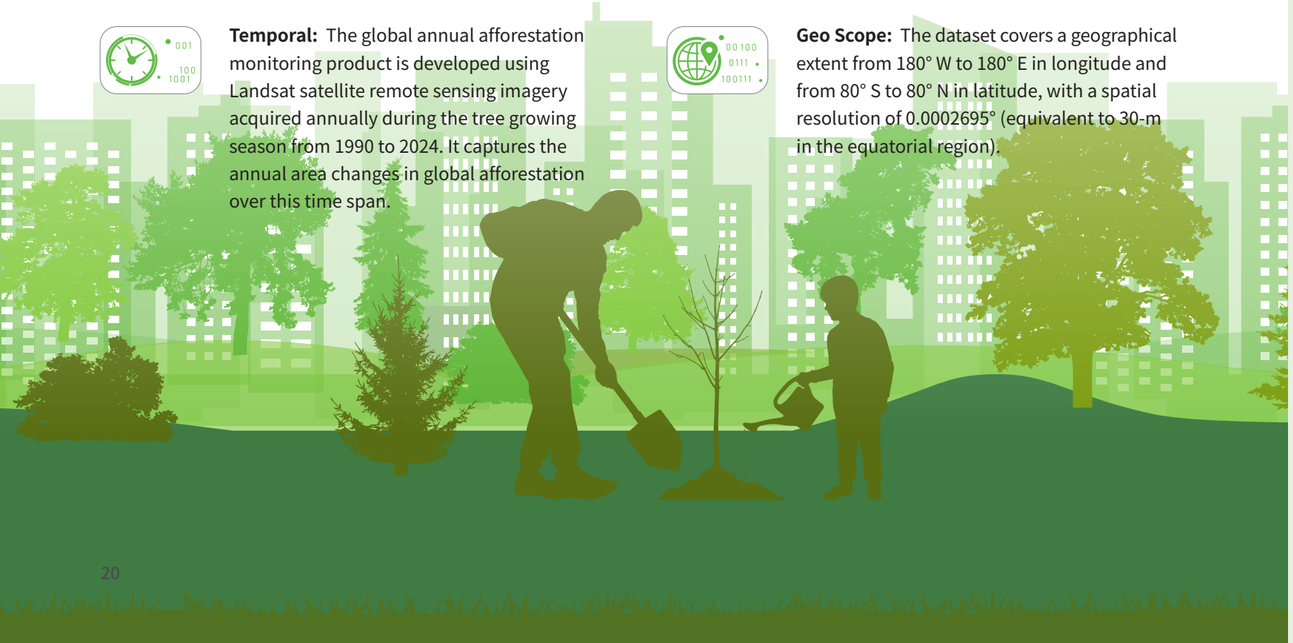
Global 30-m annual afforestation monitoring product from 1990 to 2024 (GAAM_30m_1990-2024)

Product Summary

Global afforestation areas refer to forested regions established through planting trees—excluding tree crops—for wood and fiber production or for ecosystem protection against wind and/or soil erosion (Richter et al, 2024). Afforestation is considered an important nature-based solution to address climate change, land degradation, and biodiversity loss. Consequently, countries around the world have jointly promoted afforestation through ecological restoration programs and various initiatives, making afforestation a key component in climate negotiations, carbon markets, and biodiversity strategies.

Temporal: The global annual afforestation monitoring product is developed using Landsat satellite remote sensing imagery acquired annually during the tree growing season from 1990 to 2024. It captures the annual area changes in global afforestation over this time span.

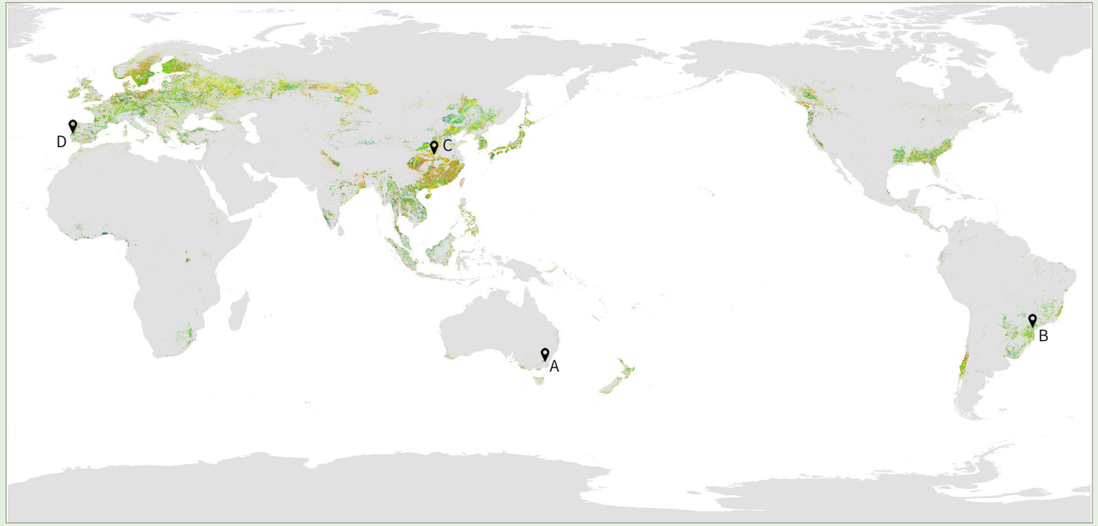
Geo Scope: The dataset covers a geographical extent from 180° W to 180° E in longitude and from 80° S to 80° N in latitude, with a spatial resolution of 0.0002695° (equivalent to 30-m in the equatorial region).



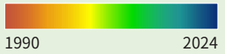
Support SDGs: SDG 15 Life on land



Global 30-m annual afforestation monitoring product from 1990 to 2024



Afforestation Year



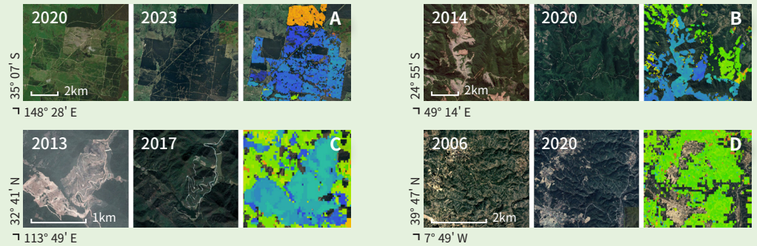
Afforestation areas

A. Tumut, New South Wales, Australia

B. Cerro Azul, Paraná State, Brazil

C. Zhumadian, Henan Province, China

D. Castelo Branco, Portugal



Methods

This data product is developed from multi-source remote sensing data using time-series analysis methods. The data sources include Landsat satellite imagery and the Spatial Database of Planted Trees Version 2.0 (SDPT V2) from the World Resources Institute (WRI) (Richter et al, 2024). First, potential global afforestation areas were delineated by integrating the spatial extent of planted forests in WRI's SDPT V2 and conducting trend break analysis of vegetation index time series. Second, Landsat imagery acquired during the tree growing season each year from 1990 to 2024 was selected to calculate the annual maximum Normalized Burn Ratio (NBR). Due to gaps in Landsat observations across certain years and regions, a sliding window strategy was applied to fill missing values, and the Whittaker Smoothing algorithm was used to denoise the NBR time series, resulting in a continuous and smooth annual NBR trajectory. Finally, the LandTrendr algorithm was employed to automatically fit and segment the NBR time series, enabling the extraction of global afforestation years via temporal breakpoint detection with prior knowledge.

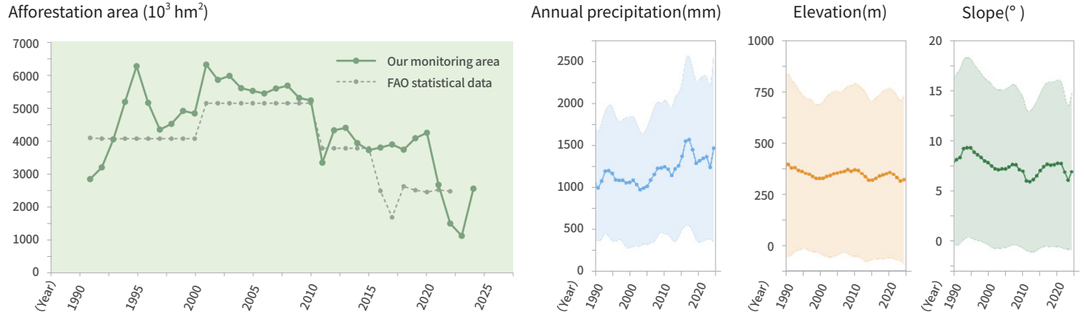
Accuracy assessment

Based on visual interpretation and the annual global afforestation and forest age maps (Cheng et al., 2023), a total of 9 216 validation samples were randomly stratified across global afforestation areas, covering different planting years and ecological zones. The identification consistency within a ±5-year margin was 82.45%, and the comprehensive F1 score reached 86.46%.



Scientific Results

Based on our product data and FAO statistics, global afforestation areas expanded before 2010 and declined afterward, showing distinct spatiotemporal heterogeneity. Activities in China, the U.S., and Europe peaked between 1990 and 2005, while those in South America (e.g., Brazil) peaked around 2010. Recently, equatorial regions—especially in Africa and Southeast Asia—have become more active. Afforestation areas are shifting from arid, high-altitude zones to humid, lowland regions with greater ecological stability. However, arid regions like the Sahel region in Africa and the dry grasslands in Central Asia still host active planting, reflecting their continued importance in large-scale restoration and climate resilience strategies despite broader global trends toward more favorable environments.



Product Details

This product adopts the WGS84 coordinate system, longitude-latitude projection (EPSG: 4326) and 30m resolution, with an output format of GeoTIFF. The product is tiled into 341 files, each covering a 10° ×10° area (~37000×37000 30-m pixels). Each tile contains a single layer/band, with values 1990-2024 indicating afforestation year.

▪ **Corresponding Authors:** Zhenrong Du, duzhenrong@dlut.edu.cn; Le Yu, leyu@tsinghua.edu.cn

▪ **References:**

1. Zhenrong Du, Le Yu, Jianyu Yang, et al. 2022. A global map of planting years of plantations. Scientific data, 9(1): 141. https://doi.org/10.1038/s41597-022-01260-2.
2. Richter J, Goldman E, Harris N, et al. 2024. Spatial database of Planted Trees (SDPT version 2.0). Technical Note. Washington, DC: World Resources Institute. Available online at: doi.org/10.46830/writn.23.00073.
3. Kai Cheng, Yuling Chen, Tianyu Xiang, et al. 2023. 2020 forest age map for China with 30 m resolution. Earth System Science Data, 16: 803–819. https://doi.org/10.5194/essd-16-803-2024.

▪ **Data Citation:**Zhenrong Du, Le Yu. Global 30m annual afforestation monitoring product from 1990 to 2024 (GAAM_30m_1990-2024), Beijing: International Research Center of Big Data for Sustainable Development Goals (CBAS), 2026. doi: 10.12237/casearth.6a86b88c2e35784b060345f3

▪ **Product URL:** http://data.casearth.cn/thematic/2025

▪ **Citation and Disclaimer for Data Use:** Users of this product shall clearly indicate the source and the authors of "Global 30-m annual afforestation monitoring product from 1990 to 2024 (GAAM_30m_1990-2024)" in all forms of their research output (including, but not limited to, published and unpublished papers/reports, theses, monographs, data products, and other academic output)generated by using this data product, and shall cite the corresponding references . The data producers shall not be liable for any loss arising from the use of this product. The boundaries and marks used in the maps do not represent an official opinion or endorsement by the data producers.

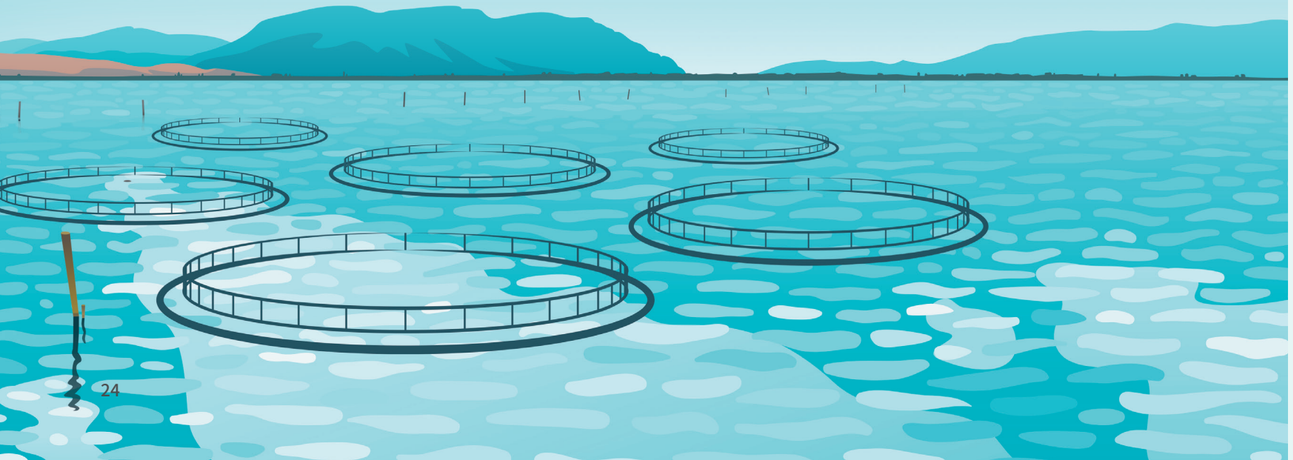
Global 30-m marine raft aquaculture data product in 2010, 2020, and 2024 (GOFAR_30m_2010/2020/2024)

Product Summary

Marine raft aquaculture refers to a production system where floating rafts are used to suspend infrastructure for cultivating aquatic organisms in shallow marine or intertidal environments. The raft aquaculture areas in this product represent the maximum distribution of various types of marine raft aquaculture facilities, including cages. The global marine raft aquaculture data product allows detailed mapping of the spatial distribution of marine raft aquaculture, revealing its distribution patterns and evolutionary trends worldwide. This achievement not only demonstrates the multi-dimensional impacts of raft aquaculture on marine food supply chains, biodiversity, and carbon cycles but also provides valuable scientific evidence for evaluating sustainable marine resource development and ecological protection policies.

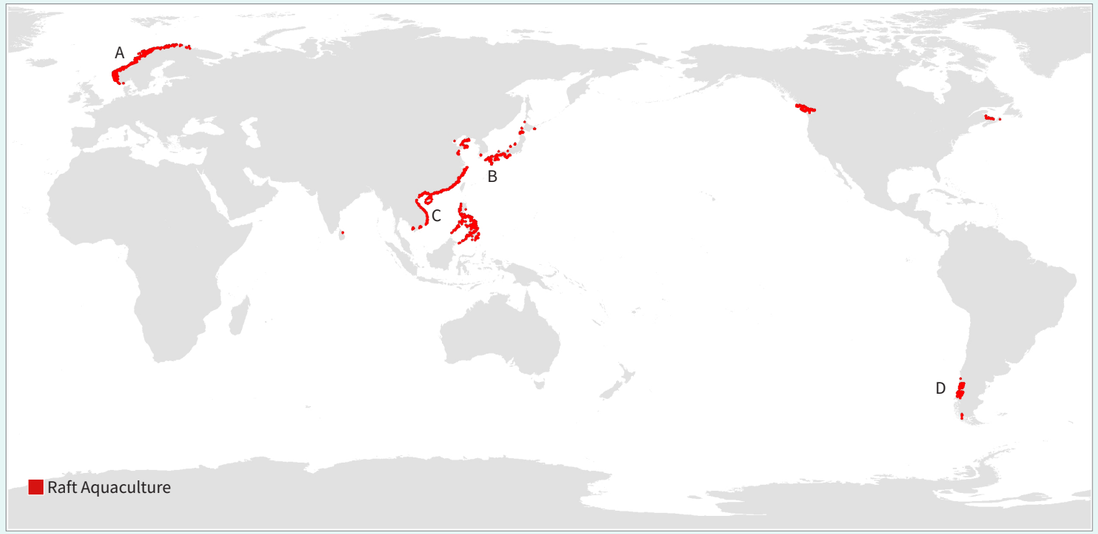
Temporal: The product is developed using satellite data such as Landsat 5/7, Sentinel-1/2, and SDGSat-1, comprising three datasets for 2010, 2020, and 2024 with an annual temporal resolution.

Geo Scope: The product covers a geographical extent from 180° W to 180° E in longitude, and from 80° S to 80° N in latitude.



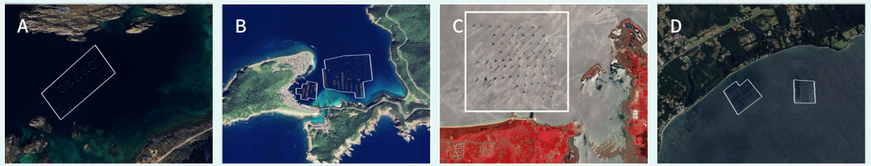
Support SDGs: SDG 14 Life below water

Global 30-m marine raft aquaculture data product in 2024



Typical aquaculture areas

A. Nordland County, Norway
B. Kochi Prefecture, Japan
C. Lingao County, China
D. Calbuco, Chile

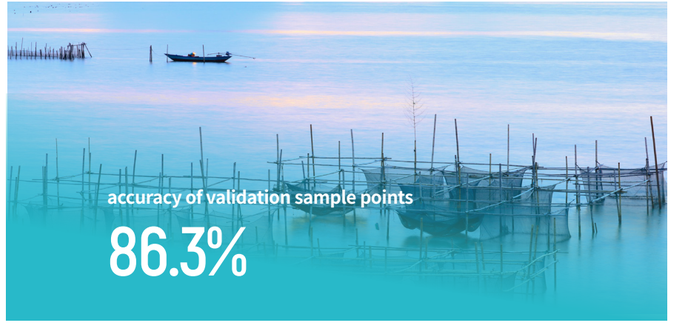


Methods

This product is a high spatio-temporal resolution dynamic monitoring product developed from multi-source satellite remote sensing data. By fusing the spectral, textural, and geometric features of time-series optical and radar imagery and combining deep learning algorithms, it enables the precise extraction of the maximum distribution of raft aquaculture facilities, including cages. The product uses a WaveNet model based on residual connections and an encoder-decoder architecture, combined with multi-temporal optical and SAR satellite imagery to extract raft aquaculture areas. The model integrates feature aggregation and dispersion modules, which not only reduce model complexity and parameter count but also significantly enhance feature representation. This method avoids the tedious process of building large-scale sample libraries and achieves higher segmentation and recognition accuracy even with limited samples. However, due to seasonal changes, water vapor conditions, and sea states, single-temporal imagery often fails to fully capture all aquaculture areas. Therefore, results from different temporal optical and SAR imagery are fused, then sorted, standardized, and revised. The fused results ultimately yield the global distribution of raft aquaculture areas, forming the annual global raft aquaculture data products (Wang Chengyi et al., 2022).

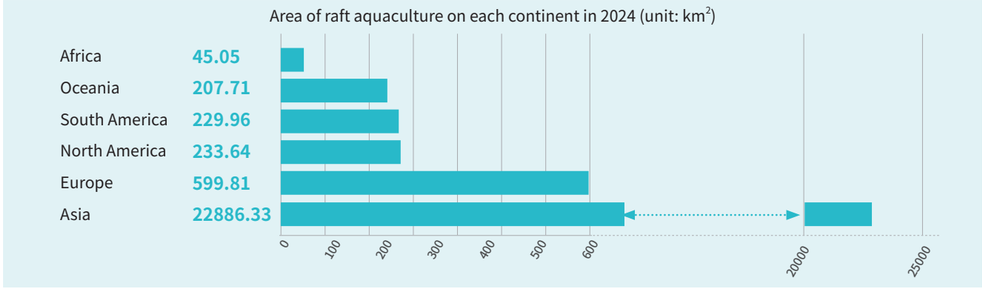
Accuracy assessment

During production, GF-1/2/3 satellite imagery was used to independently extract raft aquaculture results and perform cross-validation to meet basic accuracy requirements. Meanwhile, typical validation sample points were selected in China, and multi-temporal remote sensing data were incorporated to evaluate the accuracy of the product. The average overall accuracy across three years reached 86.3%.



Scientific Results:

As of 2024, the global raft aquaculture area reached 24 202.52 km^2, exhibiting a highly uneven spatial distribution, with Asia accounting for 94.56%. As a global leader in marine aquaculture, China's raft aquaculture area continued to expand between 2010 and 2024. Countries such as Japan, the Republic of Korea, Indonesia, the Philippines, and Vietnam have also developed large-scale raft aquaculture. From 2010 to 2024, the global marine raft aquaculture area increased by 7.15 times, with particularly significant growth in Asia, while growth in Europe was relatively modest. Although the raft aquaculture area in Africa remains limited, it has huge development potential. Developing countries like China and Vietnam primarily practice floating raft aquaculture, showing an intensive trend; while developed countries like Norway and Canada mainly adopt feed-based cage aquaculture, focusing on cultivating high-value aquatic products.



Product Details

This product adopts the WGS84 coordinate system with latitude and longitude projection (EPSG: 4326), and it is in shapefile format. The shapefile contains two main attribute fields: the "Type" field (where a value of 1 indicates the breeding area) and the "Area" field (measured in square kilometers, indicating the size of each patch).

▪ **Corresponding Authors:** Chengyi Wang, wangchengyi@aircas.ac.cn; Zujia Wang, wangzj@aircas.ac.cn

▪ **References:**
1. Chengyi Wang,Lei Wang,Ningyang Li.2025. Wave-Net-A Marine Raft Aquaculture Area Extraction Framework Based on Feature Aggregation and Feature Dispersion for Synthetic Aperture Radar Images. Sensors, 25, 2207, DOI: 10.3390/s25072207.
2. Chengyi Wang, et al. 2022. A Method for Extracting Raft Aquaculture Areas Based on Multi-temporal Optical Remote Sensing Images, Invention Patent (2022102933775).

▪ **Data Citation:**Chengyi Wang, Zujia Wang. Global 30m marine raft aquaculture data product in 2010, 2020, and 2024 (GOFAR_30m_2010/2020/2024), Beijing: International Research Center of Big Data for Sustainable Development Goals (CBAS), 2026. doi: 10.12237/casearth.6a16986388ccf41e97bb3e5f

▪ **Product URL:** http://data.casearth.cn/thematic/2025

▪ **Citation and Disclaimer for Data Use:** Users of this product shall clearly indicate the source and the authors of "Global 30-m marine raft aquaculture data product in 2010, 2020, and 2024 (GOFAR_30m_2010/2020/2024)" in all forms of their research output, including, but not limited to, published and unpublished papers/reports, theses, monographs, and data products generated by using this data product, and shall cite the corresponding references. The data producers shall not be liable for any loss arising from the use of this product. The boundaries and markings on the maps do not represent any official opinion or endorsement by the data producers.

Global 1-km soil moisture data product in 2020, 2021, and 2024(GL_SSM_1km_2020/2021/2024)

Product Summary

The Global Soil Moisture product is a high-precision remote sensing dataset generated from FY-3D satellite MERSI-II multispectral data and multi-source auxiliary datasets. By applying the XGBoost machine learning algorithm, the product deeply integrates MERSI-II multi-band observational data, ERA5-Land low-resolution reanalysis soil moisture, and static variables including topography and soil texture. This approach enables daily, global-scale monitoring of surface soil moisture, delivering essential data for precision agricultural irrigation guidance, regional drought early warning, land surface process simulation, and global water cycle studies.

Temporal: The Global Soil Moisture product covers the years 2020, 2021, and 2024, with a daily temporal resolution.

Geo Scope: The Global Soil Moisture product covers a geographic range from 180° W to 180° E and from 70° N to 60° S, with a spatial resolution of 1 km.

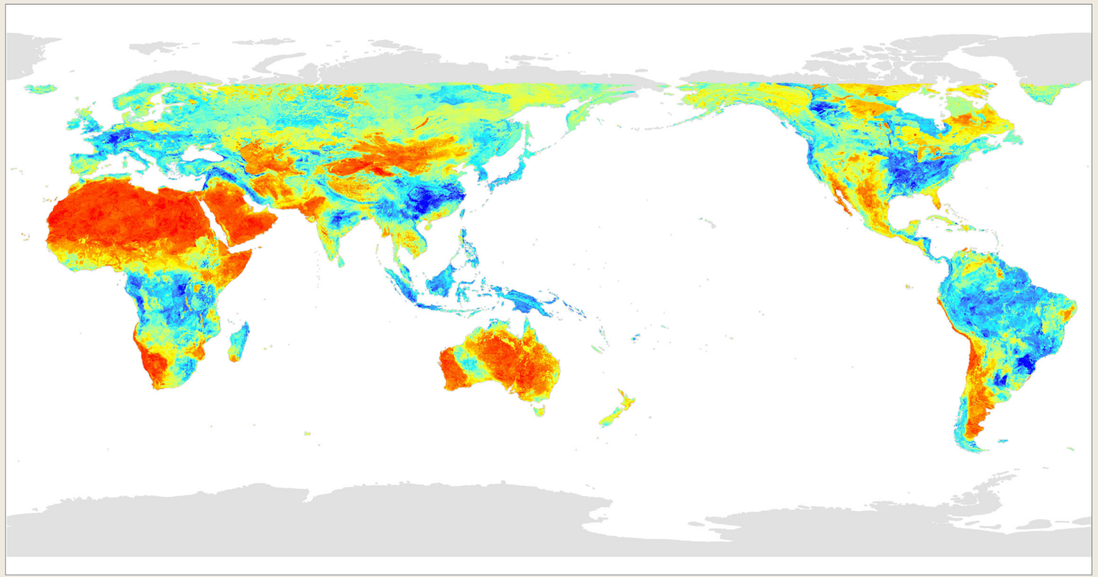




Support SDGs: SDG 2.4 Ensure sustainable food production systems
SDG 15.3 Combat desertification, restore degraded land and soil



Global Surface Soil Moisture product at 1- km resolution on January 10, 2020



volumetric water content(m^3/m^3)

0 0.6 NoData

Methods

The product is generated through the following steps: First, physical preprocessing is performed on MERSI-II data, during which DN values in the thermal infrared bands are converted to brightness temperature, and DN values in the visible/near-infrared bands are converted to reflectance. Geometric observation parameters, including the solar zenith angle, are also extracted for each pixel. Then, the ERA5 reanalysis soil moisture values and static variable values corresponding to the given date are read, and the multi-source data are assembled into a model input feature set. Second, the XGBoost machine learning model, once trained, is applied to global MERSI-II satellite data for soil moisture prediction. Finally, the retrieved results are stitched together and reprojected to produce the final global surface soil moisture product.

Accuracy Assessment

This soil moisture product is developed using the XGBoost machine learning algorithm with multi-source data fusion. Temporal validation is performed using 221 in-situ sites from nine global ISMN networks, targeting 0–10 cm topsoil moisture, with four metrics adopted: *R* (correlation coefficient), Bias, RMSE, and ubRMSE. Cross-spatial comparison is conducted against the GLASS dataset. North American networks yield median *R* values of 0.72–0.74 and negligible Bias of 0.01 m^3/m^3, while European and Australian networks achieve better consistency, with median *R* values of 0.78–0.82 and low ubRMSE of 0.03–0.05 m^3/m^3. The spatial pattern of the product matches GLASS well, with no systematic bias.



▪ **Corresponding Authors:** Xiaoping Du, duxp@aircas.ac.cn;Shunlin Liang,shunlin@hku.hk

▪ **References:**

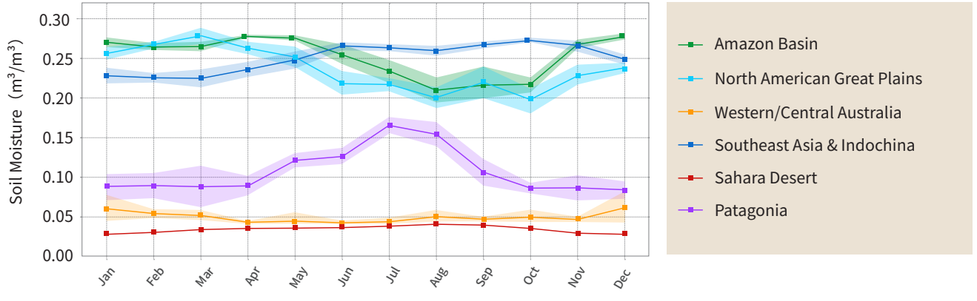
1. Yufang Zhang, Shunlin Liang, Han Ma, et al.2023.Generation of global 1 km daily soil moisture product from 2000 to 2020 using ensemble learning.Earth System Science Data, 15, 2055–2079, https://doi.org/10.5194/essd-15-2055-2023
2. Yufang Zhang, Shunlin Liang, Han Ma, et al.2025.A seamless global daily 5 km soil moisture product from 1982 to 2021 using AVHRR satellite data and an attention-based deep learning model, Earth System Science Data, 17, 5181–5207, https://doi.org/10.5194/essd-17-5181-2025

▪ **Data Citation:**Xiaoping Du,Shunlin Liang. Global 1-km soil moisture data product in 2020, 2021, and 2024(GL_SSM_1km_2020/2021/2024), Beijing: International Research Center of Big Data for Sustainable Development Goals (CBAS), 2026. doi: 10.12237/casearth.6a88114b2e35784b06034a43

Scientific Results:

Based on the monthly mean soil moisture of six typical global regions in 2020, soil moisture baselines vary significantly across climate zones and are governed by background precipitation. Tropical rainforest regions maintain soil moisture of 0.21–0.28 m^3/m^3, while arid regions remain at 0.03–0.07 m^3/m^3. Each region exhibits unique seasonal variations consistent with local precipitation patterns. The Sahara features persistently low soil moisture, demonstrating evident hydrological inertia within an extremely arid environment.

Monthly Mean Soil Moisture Variation in Global Typical Regions (2020)



Product Details

The Global Soil Moisture product uses the WGS84 coordinate system with a geographic latitude/longitude projection (EPSG:4326), and the output file format is GeoTIFF. The data are output in spatial files, with each period containing approximately 260 spatial tile files. Each tile covers a spatial extent of 10° × 10° and consists of approximately 1 000 pixels × 1 000 pixels. Each tile file contains a single layer (band). A value of -9999 represents invalid data (NoData), while all other valid values represent the actual soil moisture levels and require the application of a scale factor of 0.001.

▪ **Product URL:** http://data.casearth.cn/thematic/2025

▪ **Data Source:** FY-3D/MERSI-II satellite observations, National Satellite Meteorological Center.

▪ **Citation and Disclaimer for Data Use:** Users must clearly indicate the source and author of the "Global 1-km soil moisture data product in 2020, 2021, and 2024(GL_SSM_1km_2020/2021/2024)" in their research outcomes (including but not limited to published papers, monographs, data products, and unpublished research reports, data products, etc.) generated using this data product, and cite relevant literature. The data producer shall not be liable for any losses incurred by users due to the use of these products; the boundary or mask data used in the maps do not represent any official viewpoint or confirmation of the relevant information by the data producer.

Global 1-km aerosol optical depth data product in 2020, 2021, and 2024(GL_AOD_1km_2020/2021/2024)

Product Summary

The Global Aerosol Optical Depth (AOD) product is derived from 1 km resolution L1-level apparent reflectance data of the MERSI-II (Medium Resolution Spectral Imager-II) onboard the FY-3D satellite. It is retrieved through the Deep Blue algorithm with lookup tables (LUTs), incorporating prior surface reflectance knowledge from the MCD19A3 BRDF (Bidirectional Reflectance Distribution Function) database, global 1 km aerosol type classification data, and a digital elevation model.

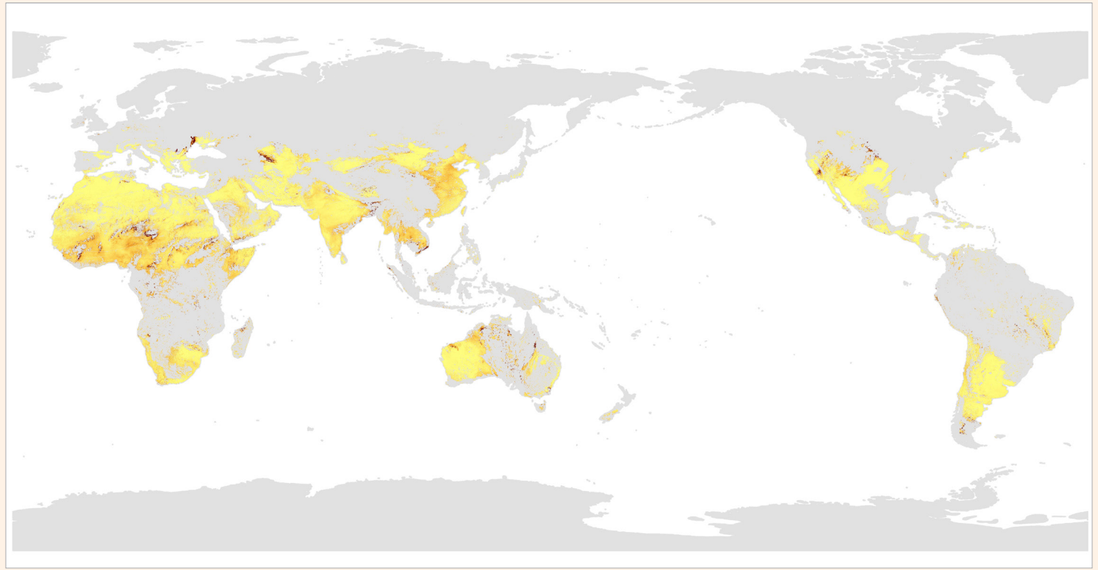
Temporal: The Global Aerosol Optical Depth product covers the years 2020, 2021, and 2024, with a daily temporal resolution.

Geo Scope: The Global Aerosol Optical Depth product covers a geographic range from 180° W to 180° E and from 60° S to 70° N, with a spatial resolution of 1-km.



Support SDGs: SDG 11.6 Reduce the adverse environmental impact of cities

Global aerosol optical depth data product at 1- km resolution on January 31, 2020



Methods

First, we read FY-3D/MERSI-II L1 HDF5 data to extract 1 km blue, red, and near-infrared reflectance, along with viewing and solar geometry. Geometric correction is performed via thin plate spline (TPS) interpolation on embedded GCPs to generate a 0.01° WGS84 lat-lon grid. We spatially and temporally resample the three Ross Thick-Li Sparse_Ri BRDF parameters from MCD19A3 to expand valid AOD retrievals and reduce errors arising from Lambertian surface assumptions. The 1 km aerosol classification data are used to define the radiative transfer models, and the DEM is applied for elevation correction. Multi-dimensional LUTs are built using the 6S model, linking blue-band reflectance to AOD via bilinear interpolation across aerosol types, seasons, BRDF, and observation geometries. A combined mask filters clear-sky pixels through blue-band thick-cloud thresholds, 3×3-window thin-cloud detection, NDVI water/cloud-shadow separation, and NDSI snow-ice screening. Pixel-wise AOD is retrieved by linearly interpolating the minimum residuals between observed and simulated reflectance, with physically invalid AOD values (-1,0] and >5 adjusted. Final spatial QC comprises 3×3 cloud-edge dilation to remove polluted adjacent pixels, 5×5 high-outlier screening, and 7×7 mean±2σ smoothing, yielding gridded AOD outputs.

Accuracy Assessment

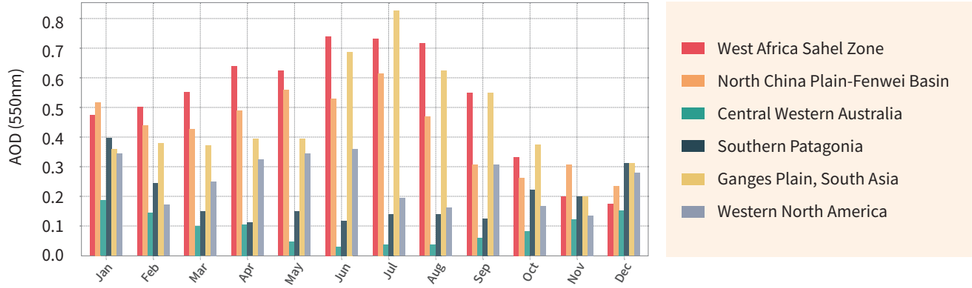
This AOD product is retrieved using the 6S radiative transfer model and a multidimensional lookup table inversion approach. Quality control is performed throughout the processing chain through cloud snow water masking and spatial filtering. Quantitative validation is conducted using time-series data from 165 AERONET L2.0 stations worldwide, and global spatial comparisons are made against the MODIS MAIAC AOD product. Spatiotemporal and spectral matching are verified, and the accuracy is evaluated using four metrics: *R* (Pearson correlation coefficient), RMSE (root mean square error), MAE (mean absolute error), and EE (expected error). A total of 21 712 valid matching samples were obtained, demonstrating excellent product accuracy: *R* reaches 0.81, RMSE=0.15，MAE=0.09，and 67.53% of the samples fall within the expected error range.



Scientific Results:

Statistical results reveal pronounced spatial-temporal disparities in aerosol optical depth (AOD, dimensionless) across six typical global regions in 2020, governed by atmospheric circulation, dust transport, and anthropogenic emissions. The Indo-Gangetic Plain exhibits the highest annual AOD, with a July peak of 0.83, driven by summer monsoons, industrial pollution, and biomass burning. The Sahel exhibits a unimodal pattern, peaking at 0.74 in June during intense Saharan dust transport. The North China Plain-Fenwei Basin reaches its maximum AOD of 0.62 in July, due to vigorous secondary aerosol formation. Central and western Australia maintains persistently low AOD (0.03–0.15). Southern Patagonia and western North America show a winter-high and summer-low AOD pattern. Standard deviations ranging from 0.08 to 0.35 indicate strong intra-regional aerosol heterogeneity.

Monthly AOD Comparison of Global Aerosol High-Value Core Regions (2020)



Product Details

This global AOD product adopts the WGS84 (EPSG:4326) geographic projection and outputs LZW-compressed GeoTIFF tiles. Each 0.01° Float32 raster tile covers a 10° ×10° region and consists of 1000×1000 pixels, with approximately 170 tiles per global dataset. Pixels store dimensionless 550 nm AOD values ranging from 0 to 5, and -9999.0 is assigned as the NoData flag.

▪ **Corresponding Authors:** Xiaoping Du, duxp@aircas.ac.cn;Shunlin Liang,shunlin@hku.hk

▪ **References:**

1. Qingxin Wang,Siwei Lib,Jie Yang, et al. 2023. A high-precision aerosol retrieval algorithm for FY-3D MERSI-II images. Environment International, 173,https://doi.org/10.1016/j.envint.2023.107841

2. Dong Zhou,Qingxin Wang,Siwei Li, et al. 2024.Preliminary Retrieval and Validation of Aerosol Optical Depths from FY-4B Advanced Geostationary Radiation Imager Images.Remote Sensing, 16(2):372,https://doi.org/10.3390/rs16020372

▪ **Data Citation:** Xiaoping Du,Shunlin Liang. Global 1-km aerosol optical depth data product in 2020, 2021, and 2024(GL_AOD_1km_2020/2021/2024), Beijing: International Research Center of Big Data for Sustainable Development Goals (CBAS), 2026. doi: 10.12237/casearth.6a8811872e35784b06034a46

▪ **Product URL:** http://data.casearth.cn/thematic/2025

▪ **Data Source:** FY-3D/MERSI-II satellite observations, National Satellite Meteorological Center.

▪ **Citation and Disclaimer for Data Use:** Users must clearly indicate the source and author of the "Global 1-km aerosol optical depth data product in 2020, 2021, and 2024(GL_AOD_1km_2020/2021/2024)" in their research outcomes (including but not limited to published papers, monographs, data products, and unpublished research reports, data products, etc.) generated using this data product, and cite relevant literature. The data producer shall not be liable for any losses incurred by users due to the use of these products; the boundary or mask data used in the maps do not represent any official view or confirmation of the relevant information by the data producer.

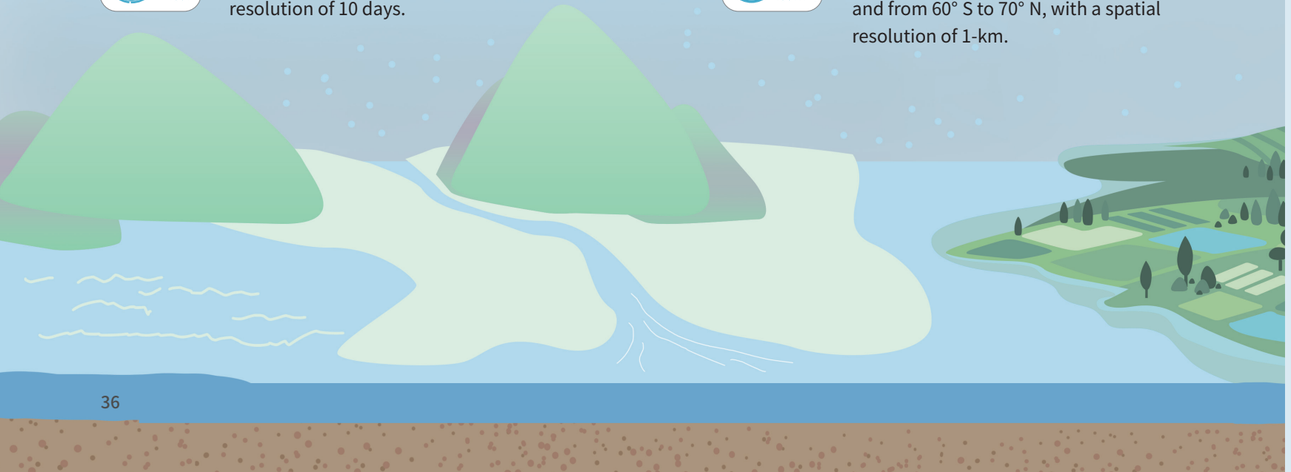
Global 1-km latent heat flux data product in 2020, 2021, and 2024(GL_LE_1km_2020/2021/2024)

Product Summary

The Global Latent Heat Flux product is based on 10-day composite NDVI data from the FY-3D MERSI L3 product. It combines the GLASS07B11 global net radiation product with MERRA-2 reanalysis meteorological data, generated through an ensemble modeling approach.This product integrates five evapotranspiration estimation models with independent physical mechanisms or statistical foundations, namely RS-PM, SW, PT-JPL, MS-PT, and Wang 2008. A linear weight set method is employed to produce the final latent heat flux result (unit: W/m^2), which enables implicit separation of the dual-source contributions from vegetation transpiration and soil evaporation. The product provides critical parameters of surface energy and water exchange for global hydrological cycle simulation, drought monitoring, and ecosystem assessment.

Temporal: The Global Latent Heat Flux product covers the years 2020, 2021, and 2024, with a temporal resolution of 10 days.

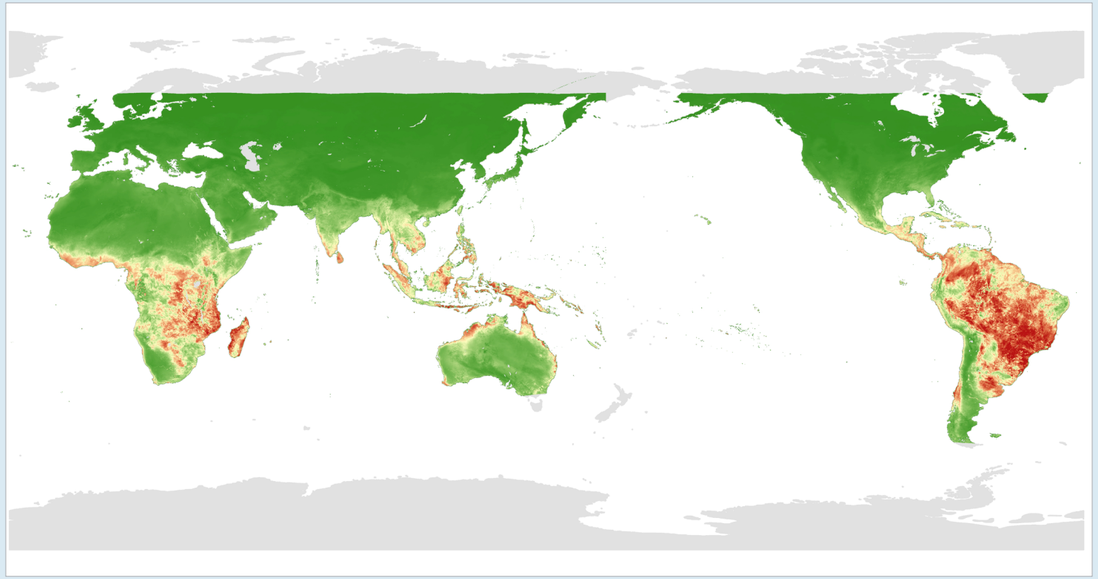
Geo Scope: The product covers a geographic range from 180° W to 180° E and from 60° S to 70° N, with a spatial resolution of 1-km.



Support SDGs: SDG 2.4 Ensure sustainable food production systems
SDG 6.6 Protect and restore water-related ecosystems
SDG 15.3 Combat desertification, restore degraded land and soil



Global Latent Heat Flux product at 1-km resolution on January 10, 2020



Methods

First, read the 10-day synthetic NDVI HDF data of FY-3D/MERSI-II L3, extract the vegetation index of 1000 m, and construct the Hammer equal area projection affine transformation matrix based on the file metadata coordinates and resolution to complete the geometric positioning. Next, read the GLASS07B11 net radiation product and convert it to net radiation at the W/m²level through a 0.01 scaling factor. Use bilinear resampling to match the 0.05° original grid to the NDVI Hammer coordinate system. Subsequently, extract hourly meteorological elements (U2M, V2M, QV2M, T2M, PS) of MERRA-2 for the three days before and after the target date, and complete the conversion from UTC to pixel local time. Calculate four meteorological parameters, including daily average temperature, daily average wind speed, daily average relative humidity, and daily temperature difference, and align them to the NDVI grid using bilinear interpolation. Using NDVI, surface net radiation, and the four meteorological elements as unified inputs, drive the five latent heat flux models (RS-PM, SW, PT-JPL, MS-PT, and Wang2008) and output five independent flux results. Finally, perform weighted ensemble fusion using weights of 0.201, 0.198, 0.191, 0.205, and 0.205 to generate a global latent heat flux product at 1 km resolution.

Accuracy Assessment

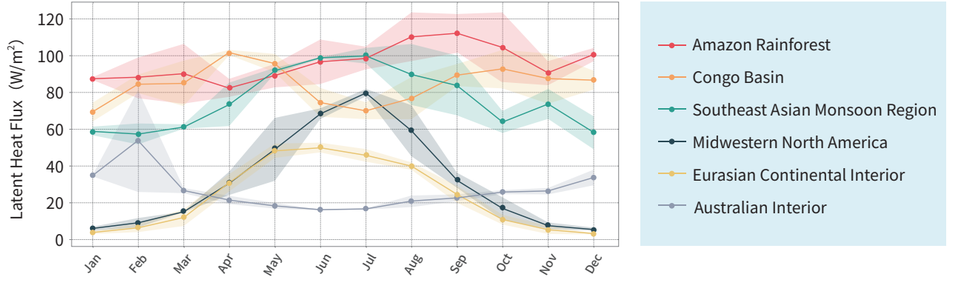
This latent heat flux product is retrieved using a Bayesian averaging algorithm. Validation is conducted using 191 global AmeriFlux and ChinaFlux eddy covariance sites across 10 land cover types, with spatial comparison against the 1 km GLASS evapotranspiration dataset. Four metrics (R^2, RMSE, Bias, and KGE) are adopted. The overall R^2 reaches 0.64 and KGE reaches 0.77; savanna achieves the optimal KGE of 0.84. RMSE ranges from 15.9 to 29.1 W/m², with negligible Bias. The global spatial pattern of the product agrees well with GLASS, with no systematic bias.The comprehensive validation precision is no less than 75%.



Scientific Results:

Based on monthly latent heat flux data for 2020, we compared seasonal evapotranspiration patterns across six typical land regions. Flux magnitude, seasonal fluctuation, and peak timing are jointly controlled by hydrothermal conditions and vegetation cover, which is consistent with global land surface energy partitioning. Equatorial rainforests maintain persistently high flux throughout the year, while tropical monsoon, temperate continental, and arid inland regions show distinct seasonal rhythms. Wet forest regions exhibit substantially higher flux than arid interiors; seasonal peak phases reverse between the hemispheres, matching regional hydrothermal regimes and vegetation phenology.

Monthly Latent Heat Flux Variation in Global Typical Terrestrial Land Regions (2020)



Product Details

The Global Latent Heat Flux product adopts the WGS84 coordinate system with geographic projection (EPSG:4326) or the Hammer equal-area global raster scene. The pixel data type is Float32 with a valid value range of 0 to 500 W/m² corresponding to surface latent heat flux. Pixels outside the valid range, as well as missing-data regions, are uniformly assigned a value of -9999 as NoData. Files are stored with LZW compression and tiled layout to reduce file size and improve reading efficiency.

▪ **Corresponding Authors:** Xiaoping Du，Shunlin Liang duxp@aircas.ac.cn

▪ **References:**

1. Yunjun Yao, Shunlin Liang, Jie Cheng, et al. 2013. MODIS-driven estimation of terrestrial latent heat flux in China based on a modified Priestley-Taylor algorithm. Agricultural and Forest Meteorology, 171-172:187-202,https://doi.org/10.1016/j.agrformet.2012.11.016
2. Yunjun Yao, Shunlin Liang, Xianglan Li, et al. 2014. Bayesian multimodel estimation of global terrestrial latent heat flux from eddy covariance, meteorological, and satellite observations. Journal of Geophysical Research: Atmospheres,119: 4521-4545.https://doi.org/10.1002/2013JD020864

▪ **Data Citation:** Xiaoping Du,Shunlin Liang. Global 1-km latent heat flux data product in 2020, 2021, and 2024(GL_LE_1km_2020/2021/2024), Beijing: International Research Center of Big Data for Sustainable Development Goals (CBAS), 2026. doi: 10.12237/casearth.6a8812b42e35784b06034a54

▪ **Product URL:** http://data.casearth.cn/thematic/2025

▪ **Data Source:** FY-3D/MERSI-II satellite observations, National Satellite Meteorological Center.

▪ **Citation and Disclaimer for Data Use:** Users must clearly indicate the source and author of the "Global 1-km latent heat flux data product in 2020, 2021, and 2024(GL_LE_1km_2020/2021/2024)"product in their research outcomes (including but not limited to published papers, monographs, data products, and unpublished research reports, data products, etc.) generated using this data product, and cite relevant literature. The data producer shall not be liable for any losses incurred by users due to the use of these products; the boundary or mask data used in the maps do not represent any official view or confirmation of the relevant information by the data producer.

Aerospace Information Research Institute, Chinese Academy of Sciences Data Use Policy for Global Sustainable Development Data Products (2025)

The Aerospace Information Research Institute, Chinese Academy of Sciences (hereinafter referred to as AIRCAS) provides unrestricted and free access to the Global Sustainable Development Data Products (2025) (hereinafter referred to as data products) in online, CD-ROM, and print formats.

Users, which include recipients of the data products and other natural persons, legal persons, or unincorporated organizations that directly or indirectly acquire, use the data products, or use any part thereof, shall be subject to this policy when downloading or using the data products.

1. Scope of Applicability

1.1 This policy applies to the data products, including but not limited to metadata, entity data files, as well as related documents, images, and research outcomes.

1.2 The provision of any copyrighted content in the data products by AIRCAS does not imply the transfer of any copyright in such content. Before using such content for specific purposes, users shall obtain all necessary permissions from the rights holder.

2. Purpose and Methods

2.1 Users may use the data products freely, on a non-exclusive basis, and free of charge for scientific research, educational, or informational purposes. These purposes include, but are not limited to, photo portfolios, theses, monographs, textbooks, public exhibitions, computer graphics simulations, web pages, and decision-making processes.

2.2 When using the data products, users shall indicate the source in the form of a dataset citation: Data from Big Earth Data Center, Chinese Academy of Sciences (http://data.casearth.cn). Under no circumstances shall users express or imply, in any manner, that the data products, related services, or activities have been endorsed or supported by AIRCAS, any of its employees, or any provider of the data products.

3. Disclaimer

3.1 All data products published by AIRCAS are provided on an "as is" and "as available" basis. Although AIRCAS takes all feasible measures and makes every effort to ensure the quality of the data products, it does not provide any explicit or implicit guarantee regarding the quality of the data products, nor does it rule out the possibility of errors. For information related to the quality of the data products, users shall refer to the relevant documents.

3.2 AIRCAS shall not be liable for any interruption in access to the data products caused by force majeure events (such as network disconnections), the withdrawal of data products by providers, administrative decisions made by Chinese administrative authorities, judicial decisions, or other objective factors. AIRCAS also reserves the right to temporarily suspend or completely terminate access to the data products at any time at its own discretion.

3.3 Under no circumstances shall AIRCAS, any of its employees, or any provider of the data products be held liable, whether directly or indirectly, to any user for any costs, expenses, claims, or demands arising from the use of the data products. This exclusion of liability applies regardless of whether the liability is based on a contract, tort, warranty, administrative decision, or judicial decision.

3.4 Neither AIRCAS, any of its employees, nor any provider of the data products shall indemnify, hold harmless, or exempt any user from liability for any form of misconduct or copyright infringement resulting from the use of the data products.

4. Legal Applicability

4.1 The establishment, validity, performance, and interpretation of this Policy shall be governed by the laws of the Chinese mainland (excluding conflict of laws provisions).

4.2 In the event that any provision of this policy conflicts with the applicable laws, the conflicting provision shall be amended or reinterpreted in accordance with the provisions of the law, while the other provisions of this policy shall remain in full force and effect.

5. Dispute Settlement

5.1 In the event of a dispute arising from this policy or the use of the data products, and if the parties involved are unable to resolve the dispute through mutual agreement, the competent courts of the Chinese mainland shall have jurisdiction over the dispute. Any party shall have the right to file a lawsuit with the competent court of the Chinese mainland, and the verdict shall be rendered in accordance with the local laws in effect at the time of the incident.

6. User Acknowledgement

6.1 Before receiving, downloading, or using any of the data products, users must have read, understood, and fully accepted all the provisions of this policy, and agree that this policy constitutes a legally binding agreement between AIRCAS and the users.

6.2 Users must ensure that their use of the data products complies with the laws of the Chinese mainland, and shall undertake not to engage in any act that violates these laws by virtue of using the data products.

Global Data Products for Sustainable Development (2025) - Authors & Members of Working Group

Global Data Products for Sustainable Development (2025) Research & Publishing Master Planning Group

Huadong Guo, Dongmei Yan, Guojin He, Jianhui Li, Xiangtao Fan, Jianbo Liu, Liangyun Liu, Xiao Zhang, Hongdeng Jian, Caihong Ma, Mingming Jia, Zhenrong Du, Chengyi Wang, Xiaoping Du

1. Global 30-m land cover dynamic monitoring product with a fine classification system from 1985 to 2022 (GLC_FCS30D_1985-2022)

Liangyun Liu, Xiao Zhang

2. Global human thermal stress index product from 2000 to 2024 (HiGTS_2000-2024)

Hongdeng Jian

3. Global industrial heat sourcedata product from 2012 to 2023(GIHS 2012-2023)

Caihong Ma

4. Global 10-m spatial distribution of mangroves in 2020 (HGMF_10m_2020)

Mingming Jia

5. Global 30-m annual afforestation monitoring product from 1990 to 2024 (GAAM_30m_1990-2024)

Zhenrong Du,Le Yu

6. Global 30-m marine raft aquaculture data product in 2010, 2020, and 2024 (GOFAR_30m_2010/2020/2024)

Chengyi Wang,Zujia Wang

7. Global 1-km soil moisture data product in 2020, 2021, and 2024(GL_SSM_1km_2020/2021/2024)

Xiaoping Du,Shunlin Liang

8. Global 1-km aerosol optical depth data product in 2020, 2021, and 2024(GL_AOD_1km_2020/2021/2024)

Xiaoping Du,Shunlin Liang

9. Global 1-km latent heat flux data product in 2020, 2021, and 2024(GL_LE_1km_2020/2021/2024)

Xiaoping Du,Shunlin Liang

Platform Construction Working Group

Xiangtao Fan, Xiaoping Du，Yihua Zheng, Qibin Lv, Hongdeng Jian, Zhenzhen Yan, Qin Zhan, Shanbo Li, Zhimin Tai, Jie Zhang

Data Sharing Publishing Working Group

Dongmei Yan, Guojin He, Zhe Zhang, Jun Yan，Xiaowei Wang,Xiaomei Wang，Yanjie Gu，Lili Guo, Yayang Lu，Ying Sun

CBAS Global Data Products for Sustainable Development (2025) - List of Consulting Experts

Le Yu, Dongping Ming, Hongyu Chen, Tao Pei，Juanle Wang, Gensuo Jia, Yunhao Chen, Wenhui Kuang, Nan Xu, Shengchao Peng, Hui Liu, Yi Zeng, Kai Yan, Fuli Yan, Lei Wang



International Research Center of Big Data for Sustainable Development Goals
Address: No. 9 Dengzhuang South Road, Haidian District, Beijing
Postal code: 100094
Telephone: +86 10 82177601
E-mail: datasharing@cbas.ac.cn
Map Approval Number: GS(2026)2162